Dual-View Microscopy with a Single Camera:
Real-Time Imaging of Molecular Orientations and Calcium

Kazuhiko Kinosita, Jr.,* Hiroyasu Itoh,‡ Shin'ichi Ishiwata,§ Ken'ichi Hirano,‡ Takayuki Nishizaka,§ and Tsuyoshi Hayakawa‡

*Department of Physics, Faculty of Science and Technology, Keio University, Hiyoshi 3-14-1, Kohoku-ku, Yokohama 223, Japan; ‡Tsukuba Research Laboratory, Hamamatsu Photonics K. K., Tokodai 5-9-2, Tsukuba-shi, Ibaraki 300-26, Japan; and §Department of Physics, School of Science and Engineering, Waseda University, Okubo 3-4-1, Shinjuku-ku, Tokyo 169, Japan

Abstract. A new microscope technique, termed "W" (double view video) microscopy, enables simultaneous observation of two different images of an object through a single video camera or by eye. The image pair may, for example, be transmission and fluorescence, fluorescence at different wavelengths, or mutually perpendicular components of polarized fluorescence. Any video microscope can be converted into a dual imager by simple insertion of a small optical device. The continuous appearance of the dual image assures the best time resolution in existing and future video microscopes. As an application, orientations of actin protomers in individual, moving actin filaments have been imaged at the video rate. Asymmetric calcium influxes into a cell exposed to an intense electric pulse have also been visualized.

OPTICAL microscopy provides a wealth of information about cellular and molecular processes. Recent development of video-based imaging technology and many purpose-oriented dyes already allow time-resolved imaging of low-contrast structures, specific molecules or ions, pH, membrane potential, et cetera (Inoué, 1986; Taylor et al., 1986; Herman and Jacobson, 1990). Analysis of molecular interplay in cells would be further aided if two (or more) of these separate images, each containing different information, are obtained simultaneously. Dual imaging is also a prerequisite in many techniques, such as the visualization of ions and pH, in which the required information resides in the ratio or difference between two images. Here we report a simple optical device that can convert any video microscope into a real-time dual imager.

Materials and Methods

Principles of W Microscopy

Fig. 1 describes the principle of our imaging technique, which we call double-view (because two images appear side by side in a single view port) or "W" (double view video) microscopy. Suppose that the image-forming beam from the sample consists of two components, shown in solid and dashed lines in Fig. 1, differing in color or direction of polarization. In conventional microscopy (Fig. 1 *A*), the two components converge at the same point making overlapping images. In W microscopy (Fig. 1 *B*), a beam splitter is inserted, preferably in a place where the beam is parallel, such that the two components deviate from each other by a few degrees. The two components then form separate images, side by side, differing in color or polarization. Dual-color or dual-polarization imaging is thus straightforward. Simultaneous observation of transmitted (including phase and differential-interference contrasts) and fluorescence images has also been achieved by separating them on the basis of color.

If the beam splitter is inserted between the objective and eyepiece (internal configuration), the two images can simultaneously be observed by eye or recorded with a video camera through the eyepiece. Alternatively, if only video recording suffices, the splitter can be placed outside the microscope body before the video camera (external configuration). A Zeiss microscope allows both configurations (see below), whereas the latter, external configuration is applicable to any video microscopes.

Among the various types of dual-image microscopy (e.g. Spring, 1990), the major advantage of the present method is the truly simultaneous acquisition of the two images. There is thus no inherent limit in time resolution. Combined with a pulsed laser fluorescence microscope (Kinosita et al., 1988), for example, the image pair can be obtained in a single, submicrosecond exposure. The dual-camera method of Inoué (1986, Figs. 5-35) or Foskett (1988) also captures two different images simultaneously. Here the advantage of W microscopy is in its economy and universality. A single camera and an ordinary, single-input image processor suffice. Moreover, W microscopy can multiply the capabilities of even more sophisticated systems. For example, a burst of pulsed excitations can be used together with a multiformat framing camera (Itoh et al., 1990) to obtain sequential, dual images separated by microsecond intervals. Extension of W microscopy to triple or quadruple imaging is also straightforward.

Configurations of the Beam Splitter Assembly

Of many possible ways of designing the beam splitter assembly, the one which we use outside the microscope body (external configuration) is shown in Fig. 2 *A*. The chevron-type splitter in which each beam hits the dichroic mirror twice assures a sharp separation by color. W polarization microscopy is achieved by replacing the dichroic mirrors with a pair of polarizing beam splitter cubes. In either case, the splitter is placed in the parallel beam between the pair of lenses that project the intermediary image formed by the microscope objective onto a video camera. On the intermediary image plane, a rectangular slit is placed that defines the edges of the pair of images so that they can be positioned side by side without overlapping. The position of this slit depends on the make of the microscope. With a Nikon TMD (Nikon Co., Ltd., Tokyo, Japan) which we have tested, an adjustable slit can be attached directly at the camera port. In a Zeiss ICM-405 (Carl Zeiss, Tokyo, Japan), which we have also tested, the intermediary image is formed
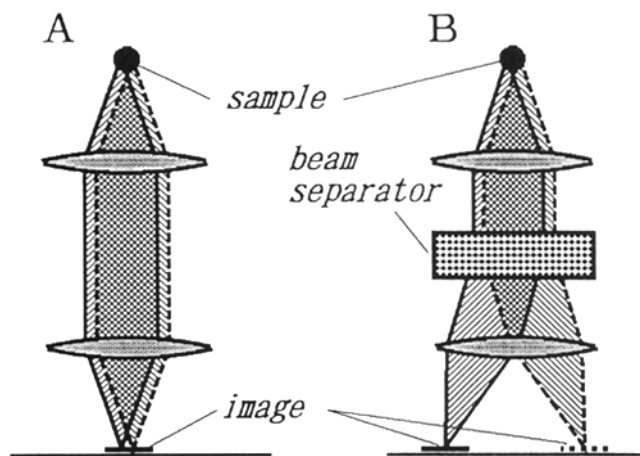
Figure 1. (*A*) Ordinary microscopy and (*B*) W microscopy. Solid and dashed lines represent two beam components differing in color or polarization.

inside the microscope body. This image plane is usually occupied by a removable scale plate, which can be replaced with an adjustable slit made for W microscopy. In this particular microscope, the output beam from the movie port is already parallel, so that we can eliminate the first lens in Fig. 2 *A*. For microscopes in which the intermediary image is not accessible from outside, an additional relay lens is required to form a secondary image, on which the slit is placed. This last method is applicable to any microscope; a universal device can be made in this way.
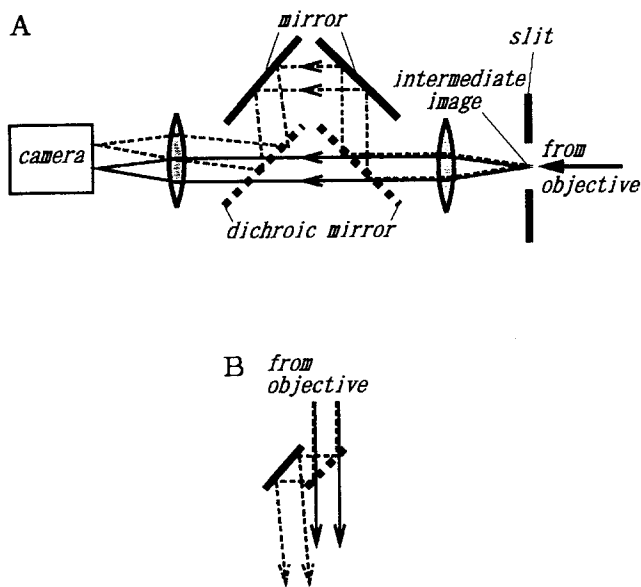
Figure 2. (*A*) A beam splitter assembly for external configuration. For polarization, the dichroic mirrors are replaced with a pair of polarizing beamsplitter cubes. Direction of the reflected beam (*dashed lines*) is adjusted by inclining the mirrors with screws. One mirror can be deflected in two directions and the other in one direction; the additional two degrees of freedom are for the restoration from a skewed beam configuration which results in image rotation. Removal of the dichroic mirrors and a slight shift of the camera position restores conventional, single-image microscopy. (*B*) A beam splitter assembly for internal configuration with a Zeiss inverted microscope. The assembly is inserted in the slot for a filter holder located immediately below the epifluorescence cassette. The inclination of the deflection mirror can be adjusted from outside with long screws.

With the Zeiss ICM-405, a small splitter shown in Fig. 2 *B* can be inserted in the microscope body below the epifluorescence cassette. In this internal configuration, the dual image can be seen by eye as well as through the camera. In this case, the image edges are defined by confining the illumination beam: a rectangular slit is placed at the position of the field diaphragm of the illumination system. Normally we prefer the external configuration, in which the adjustment of the splitter and slit is more convenient and precise.

Image Processing

Quantitative comparison, or arithmetic operation, between the pair of images obtained by W microscopy requires preprocessing of the images. In particular, the correction for image distortion, which is inevitable with a highly sensitive camera, is essential before a pixel-to-pixel comparison is attempted. We make the distortion correction by imaging a regular grid. A fine grid placed at the sample position is used for a rigorous correction, whereas a coarse grid on the intermediary image has been found satisfactory and more convenient in most situations. In either case, the dual image of the grid is approximated by a square lattice covering the whole image plane, and the vectors representing the difference are stored in a frame memory for subsequent correction of sample images. Correction vectors for pixels that do not fall on a grid corner are calculated by interpolation. Since this procedure maps the dual image of the grid onto a single, continuous lattice, the corrected image consists of an image pair aligned perfectly parallel and side by side. The constant offset between corresponding pixels, a multiple of the lattice spacing, is automatically determined.

Correction for shading is also important when the ratio of the images pair is calculated. This correction is made in the usual way by imaging a homogeneous sample, a fluorescent solution for fluorescence mode or a blank coverglass for transmission.

Subsequent to these corrections, arithmetic operations, e.g., the ratio operation, between the image pair can be performed pixel by pixel in a straightforward manner. The constant offset between the pixel coordinates has been determined in the distortion correction above. If the predetermined offset value fails, e.g., by a drift in the optical system, the failure is immediately clear for samples with defined edges such as the actin filaments and eggs shown below: even for an error of one pixel unit, the image after the ratio operation looks like one in the differential-interference contrast, one side being dark and the other side bright.

Muscle Proteins

Muscle proteins were extracted from rabbit leg and back white muscles. Actin was prepared as described previously (Masai et al., 1986). Labeled F-actin (0.1 mg/ml) was obtained by polymerizing G-actin in a solution containing 0.1 M KCl, 2 mM MgCl$_2$, 0.1 mM ATP, 2 mM MOPS (pH 7.0), and 1.5 mM NaN$_3$ in the presence of a slight molar excess of phalloidin-tetramethylrhodamine (Molecular Probes, Inc., Eugene, OR) at 0°C overnight. Unbound dye was removed by passing the solution through a small Sephadex G-25 column. Myosin was prepared as described previously (Kinosita et al., 1984) except that 1 mM DTT was added at a final stage of preparation. Heavy meromyosin (HMM)[1] was prepared according to Weeds and Pope (1977) with slight modifications: 33 mg/ml of myosin in 0.6 M NaCl, 20 mM MOPS (pH 7.0), 1 mM MgCl$_2$, and 1 mM DTT was treated with 0.5 mg/ml of α-chymotrypsin (Cooper Biomedicals, West Chester, PA) at 25°C for 8 min and the proteolysis was terminated with 0.5 mM PMSF. After dialysis against 40 mM KCl, 5 mM MOPS (pH 7.0), and 1 mM DTT, the solution was ultracentrifuged and the supernatant (10 mg/ml) was used as an HMM preparation without the ammonium sulfate fractionation. Small aliquots of the HMM solution were preserved in liquid nitrogen and used after quick thawing.

Observation of Moving Actin Filaments

Sliding motion of actin filaments over HMM was observed as described by Toyoshima et al. (1987). A chamber for the observation on the inverted microscope (Zeiss ICM-405) was made of a large and a small coverglass slip, one of which was coated with nitrocellulose (0.1% collodion). Heavy meromyosin, 50 μg/ml in a standard buffer containing 25 mM KCl, 25 mM imidazole-HCl (pH 7.4), 4 mM MgCl$_2$, and 1 mM EGTA was introduced in the chamber, followed by 0.5 mg/ml of BSA (Sigma Chemical Co., St. Louis, MO) and then by labeled F-actin diluted to 10 nM in the standard

---

1. *Abbreviations used in this paper*: HMM, heavy meromyosin.

buffer. Images of rigor filaments were taken after flushing the chamber with a deoxygenated solution, the standard buffer containing, in addition, 4.5 mg/ml of glucose, 0.22 mg/ml of glucose oxidase (Sigma Chemical Co.), 0.036 mg/ml of catalase (Sigma Chemical Co.), and 10 mM DTT. 4 mM ATP was added to the flushing solution to initiate sliding.

Free Brownian motion of actin filaments was observed in a similar chamber without the nitrocellulose coating. To prevent the adsorption of the filaments on the glass surface, the chamber was first perfused with 0.5 mg/ml of BSA. Then, the deoxygenated solution above containing labeled F-actin (10 nM) was introduced. Actin filaments decorated with excess heavy meromyosin were examined in the same way. In this case, 10 μM of labeled F-actin was preincubated with 70 μM of HMM. The sample was diluted 1,000-fold in the deoxygenated solution containing 2 μM of HMM, and introduced in the chamber.

Sea Urchin Eggs

Unfertilized eggs were collected from the sea urchin *Hemicentrotus pulcherrimus* by intracoelomic injection of 0.5 mM acetylcholine in a normal sea water (0.42 M NaCl, 9 mM KCl, 10 mM CaCl₂, 25 mM MgCl₂, 25 mM MgSO₄, and 1 mM Na₂SO₄; pH adjusted to 8.2 with NaHCO₃). The eggs were microinjected with 0.05 volume of 2 mM indo-1 (Dojindo Laboratories, Kumamoto, Japan) solubilized in water. Microinjection was performed in a Ca²⁺-free sea water (0.435 M NaCl, 9.25 mM KCl, 25 mM MgCl₂, and 25 mM MgSO₄; pH adjusted to 8.2 with NaHCO₃), and 5 min later the egg was transferred into the normal sea water (Hirano and Ishikawa, 1979). An injected egg immersed in a large droplet of the normal sea water on a coverglass was imaged on the inverted microscope (Zeiss ICM-405). For electroporation, a square-wave electric pulse was applied to the egg through a pair of platinum wires (0.3 mm diam) immersed in the droplet.

Fluorescence Imaging

All results reported in this paper were obtained with the Zeiss ICM-405 microscope in the external configuration. For W polarization microscopy of rhodamine-stained actin filaments, the fluorescence was excited at 546 nm and emission above 575 nm was detected through a 100× objective (Zeiss Neofluar). An epifluorescence dichroic mirror (Omega Optical, Inc., Brattleboro, VT) showing little polarization dependence for these wavelengths was used. The splitter assembly (Fig. 2 A) consisted of a pair of dielectric polarizer cubes and a pair of highly reflective dielectric mirrors, both covering the wavelength region of 520–800 nm (Sigma Koki Co., Ltd., Hidakamachi, Saitama, Japan). The two, orthogonally polarized images were captured side by side on an intensified (model KS1381; Video Scope International, Dulles International Airport, Washington, DC) CCD camera (model C2400-77; Hamamatsu Photonics K. K., Hamamatsu, Japan) and stored in a digital frame memory in an image processor (model C2000; Hamamatsu Photonics). Each image was corrected for background (image of a solution-filled chamber without actin), and for distortion and shading (see Image Processing above). Finally the image was spatially smoothed once (averaging over three by three pixels, one pixel unit corresponding to ~0.2 μm).

For W color microscopy of an egg loaded with indo-1, the fluorescence was excited at 340 nm and emission >390 nm (actually >410 nm, when the transmittance of the microscope and the sensitivity of the intensifier are taken into account) was observed through a 20× objective (Nikon Fluor). The dichroic mirrors in the splitter assembly had a separation wavelength at 455 nm (Kawai Kogaku, Co., Ltd., Gotenba, Japan), and aluminum mirrors were used for deflection. Background image was taken in a region close to the egg; autofluorescence of the eggs was sufficiently low compared with the indo-1 fluorescence.

Results and Discussion

Actin Orientation Revealed by W Polarization Microscopy

As an application of W microscopy, we imaged molecular orientations via polarized fluorescence. Actin filaments were visualized with the fluorescent stain phalloidin-tetramethylrhodamine. When excited with unpolarized light (virtually isotropic excitation because of the high numerical aperture

of the objective of 1.3) and viewed with W polarization microscopy, the fluorescence was clearly polarized along the axis of the actin filament as shown in Fig. 3 *A*. In Fig. 3 *B*, the polarization of fluorescence is shown in false color. The color represents the orientation of the emission transition moment of the dye at the time of observation; an orientation closer to the vertical axis of the figure is shown in red, and a horizontal orientation is shown in violet. Clearly the dye molecules are aligned along the filament axis.

This alignment implies a rigid attachment of the dye to actin. In fact, the fluorescence anisotropy of a random suspension of stained filaments was as high as 0.32 (excitation at 546 nm, emission at 590 nm; standard cuvette measurement in a Hitachi F-4010 spectrofluorometer, Hitachi Ltd., Tokyo, Japan), indicating that the half angle of dye wobble on the protein, when modeled as a motion within a cone (Kinosita et al., 1977), should be <25°. Therefore, the color in Fig. 3 *B* also serves as a marker of the orientation of individual actin protomers in the filament. Actually the color represents the average orientation of the order of 10^2 protomers lying in the length of the order of the wavelength of the fluorescence (1-μm filament contains 363 protomers).

Actin Orientation in Moving Actin Filaments

The actin filaments in Fig. 3 *B* were bound to HMM adsorbed onto nitrocellulose-coated glass. When ATP was added, the filaments started to slide over HMM as shown in Fig. 3 *C*. This motion is an in vitro model of the sliding motion that takes place in a muscle when it contracts (Toyoshima et al., 1987; Harada et al., 1987). An important question here is whether the actin protomer rotates with respect to the filament axis during the generation of sliding force. It has been suggested that actin rotation might constitute the power stroke that pulls the actin and myosin towards each other (Huxley and Simmons, 1972).

Rotation of actin protomers toward or off the filament axis should show up as a change in the polarization of the fluorescence. The change would be largest for those parts of the filaments that lie parallel with one of the two polarization axes (vertical or horizontal in Fig. 3). Consequently we compared the polarization of the vertical or horizontal part of sliding filaments (Fig. 3 *C*) with that of filaments rigidly bound to HMM (*B*), or free in solution (*D*). (Note that the speed of motion in Fig. 3, *C* and *D* would be too rapid for alternate imaging techniques, in which the two polarized components are recorded serially with a time difference of at least 33 ms). As seen in Fig. 3, *B–D*, the polarization (color) did not differ appreciably amongst the three filament states. It appears therefore that a large amplitude rotation of actin protomers does not take place during active sliding.

Quantitative Analysis of Polarization

The angle θ between the transition moment of the dye and the filament axis can be estimated from the polarization of the vertical or horizontal filaments. Owing to the isotropic excitation, the polarization, or the color in Fig. 3, is a function only of the inclination angle θ and its distribution. The relation is shown in Fig. 4, where the angular distribution is modeled as being uniform within a cone. The conical distribution represents either the orientational distribution of each dye molecule with respect to the filament axis (Fig. 4
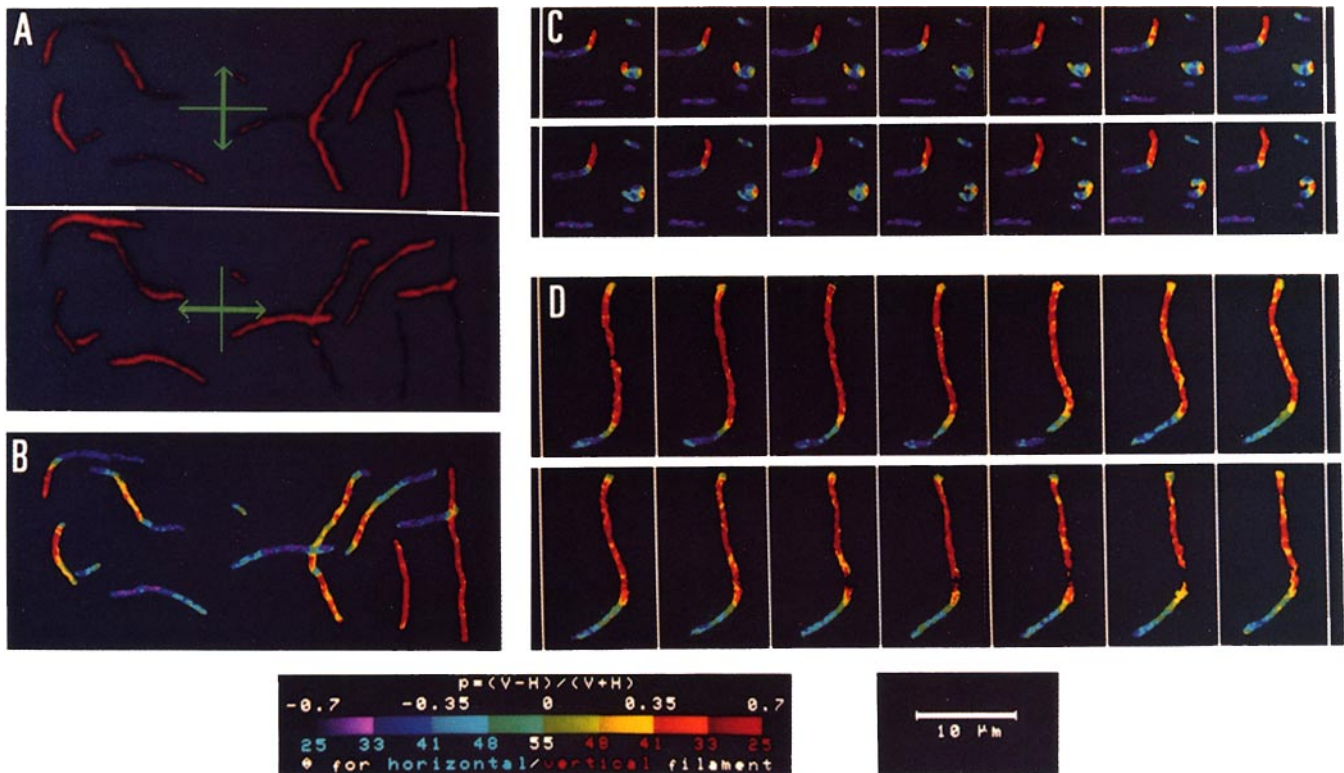
Figure 3. (*A*) Polarized fluorescence images of actin filaments stained with tetramethylrhodamine phalloidin. The filaments were bound by HMM lying on a nitrocellulose-coated coverglass. Arrows indicate the directions of polarization. (*B*) Polarization of fluorescence calculated from *A*. (*C*) Polarization images of sliding actin filaments at 33-ms intervals. 4 mM ATP was added to *A*. (*D*) Polarization images, at 33-ms intervals, of an actin filament undergoing Brownian motion in solution. In several images in *D*, part of the filament went out of focus. Scale bar applies to *A–D*; color bar applies to *B–D*. *p*, polarization; *V* and *H*, vertically and horizontally polarized components of fluorescence; θ, inclination angle in degrees (see text and Fig. 4). Temperature, 24°C.

A), or a possible filament winding not resolved in the image (Fig. 4 *B*), or the sum of these two effects.

The numbers below the color bar in Fig. 3 show the inclination angle θ for the case of no angular spread. An examination of the snap shots of several tens of filaments, including those in Fig. 3, *B–D*, indicated that this angle was well within $31 \pm 6°$, whether the filament was bound to HMM (*B*), sliding (*C*), or free in solution (*D*). Within this experimental precision we did not detect myosin-induced rotation of actin protomers. As shown in Fig. 4 *C*, however, a decrease in θ (reorientation toward the axis) and a wider angular spread have opposite effects on polarization. Exact cancellation of these two effects therefore remains as a remote possibility.

Myosin Does Not Induce Large Reorientation of Actin

It is conceivable that, under the conditions of Fig. 3, *B* and *C*, not every actin protomer necessarily interacted with the HMM which lay on the flat surface. We therefore examined samples in which actin filaments free in solution were decorated with an excess of HMM in the absence of ATP. Again, the polarization was indistinguishable, to the precision above, from that in the other samples.

We conclude from W polarization microscopy observations of individual actin filaments that the myosin-induced protomer reorientation either toward or off the filament axis is at most several degrees. Actin reorientation as the basis

of force generation seems unlikely. Prochniewicz-Nakayama et al. (1983) have reported that the fluorescence polarization of muscle fibers labeled with the actin stain phalloidin-fluorescein changed slightly upon transition of the fiber from the relaxed state to rigor or to contraction. Reorientations by a few degrees, estimated in their analysis, are not inconsistent with our observations. Note, however, that a large-scale rotation that might take place as a brief transient is yet to be examined.

Calcium Imaging by W Color Microscopy

As a second application, we obtained time-resolved images of intracellular free calcium concentration, $[Ca^{2+}]_i$, by W color microscopy. A sea urchin egg was injected with the fluorescent dye indo-1 (Grynkiewicz et al., 1985). The fluorescence of this dye is greenish at low $[Ca^{2+}]_i$ and turns bluish at high $[Ca^{2+}]_i$. By imaging the green and blue components of the fluorescence simultaneously and taking their ratio, we could follow rapid changes of $[Ca^{2+}]_i$ at the video rate of 30 frames/s (Fig. 5). Alternate (serial) imaging techniques, as used for the dye fura-2 (Tsien, 1988), would at best be half as fast.

Ca^{2+} Influx into Electroporated Eggs

Fig. 5 shows the time course of Ca^{2+} influx into an egg that was exposed to an intense electric pulse at time zero.

A

B

C

ϕ (°)

θ (°)

p=0.875

p=0.7

p=0.525

p=0.35

p=0.175
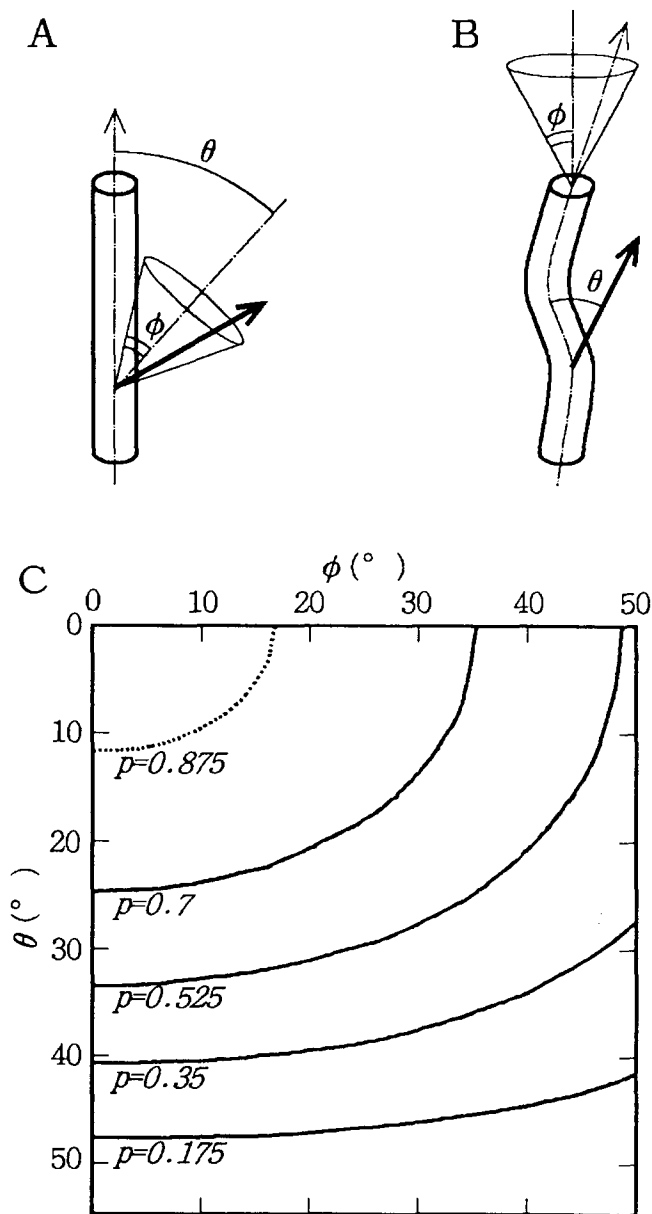
Figure 4. Dependence of the fluorescence polarization of a vertical filament on the dye inclination (θ) and its distribution (ϕ). (*A*) A model in which the angular distribution is attributed to the dye (or actin protomer) wobble. The emission transition moment of the dye (thick arrow) wobbles uniformly within a cone with a half angle ϕ. (*B*) A winding filament model in which the inclination of each dye is fixed but the filament axis wobbles in the cone. This model gives the same angular distribution as in *A*. (*C*) Polarization contours in the θ–ϕ plane. p (*polarization*) = 0 for $\theta = 54.7°$. Contours for a horizontal filament are the same except for the change of sign of p values. Zones separated by solid curves are color coded in Fig. 3. Polarization was calculated for a stretch of filament consisting of a helical array of actin protomers. Excitation was assumed to be isotropic (oscillation in all directions). Depolarization of emitted fluorescence due to the large numerical aperture of the objective (1.3) was taken into account as described by Axelrod (1979).

Such a pulse treatment is known to cause "electroporation," or transient permeabilization of the cell membrane (Zimmermann, 1982; Tsong, 1983; Neumann et al., 1989). Measurements of the transmembrane potential have indicated that, during a microsecond pulse treatment, the two regions of the cell membrane facing the positive and negative electrodes are almost equally permeabilized (Kinosita et al., 1988; Hibino et al., 1991).

As expected, Ca^{2+} influxes were seen on the positive and negative sides (Fig. 5). These fluxes were very rapid: Ca^{2+} traveled tens of microns in 1 s, implying a diffusion coefficient of the order of 10^{-6} cm²/s, a value close to that for free diffusion in water. By 1 min a low $[Ca^{2+}]_i$ was restored, showing both membrane resealing and the presence of efficient Ca^{2+} sequestering mechanisms in the egg. The termination of the Ca^{2+} influxes before they reached the center of the egg can also be explained by the competition with the sequestering system.

A closer look at Fig. 5 reveals that Ca^{2+} influxes on the positive- and negative-electrode sides were asymmetric, an unexpected finding. Initially the influx from the positive side was higher, but the tendency was reversed at $\sim$1 s. The rise in $[Ca^{2+}]_i$ resulted in the partial elevation of the fertilization envelope (Fig. 5, *bottom right*). This elevation was also asymmetric: when the initial Ca^{2+} influx from the positive side was large enough, the envelope on the positive side was larger, although the cumulative Ca^{2+} influx was higher on the negative side (Fig. 5). A shorter electric pulse induced Ca^{2+} influxes similar to those in Fig. 5 except for smaller magnitudes on both sides (not shown). In this case the envelope was observed mainly on the negative side. In the Ca^{2+}-free sea water (2 mM EGTA added), neither Ca^{2+} influxes nor envelope elevation was observed.

Apparently the pulse treatment did not impair the viability of the eggs. When an egg treated with a 400 V/cm, 400-μs pulse was inseminated 3 min later, the fertilization envelope was formed on the remaining surface where the envelope had not elevated after the electroporation. The cortex retained the potential to induce cortical exocytosis. Furthermore, this embryo continued to develop normally through the blastula stage.

Asymmetry in Electroporation

Electrophoretic accumulation of Ca^{2+} under the membrane facing the positive electrode during the pulse treatment might explain the rapid initial influx from this side. The larger total influx on the negative side appears to be due to a slower resealing of membrane on this side. Although these explanations are tentative, the present finding sheds some light on the asymmetry of electroporation, a subject that is still being debated: while the induced permeability during the microsecond electric pulse appears largely symmetric as mentioned above, later effects, passage of ions or molecules across the membrane or secondary effects thereof, have often been reported to occur on only the positive or negative side (Rossignol et al., 1983; Mehle et al., 1985; Sowers, 1988). With sea urchin eggs, in particular, Rossignol et al. (1983) observed partial fertilization envelope on the positive side, whereas Hibino et al. (1991) found it on the negative side. We can now offer an explanation of this discrepancy since the former used a long electric pulse whereas the latter a shorter
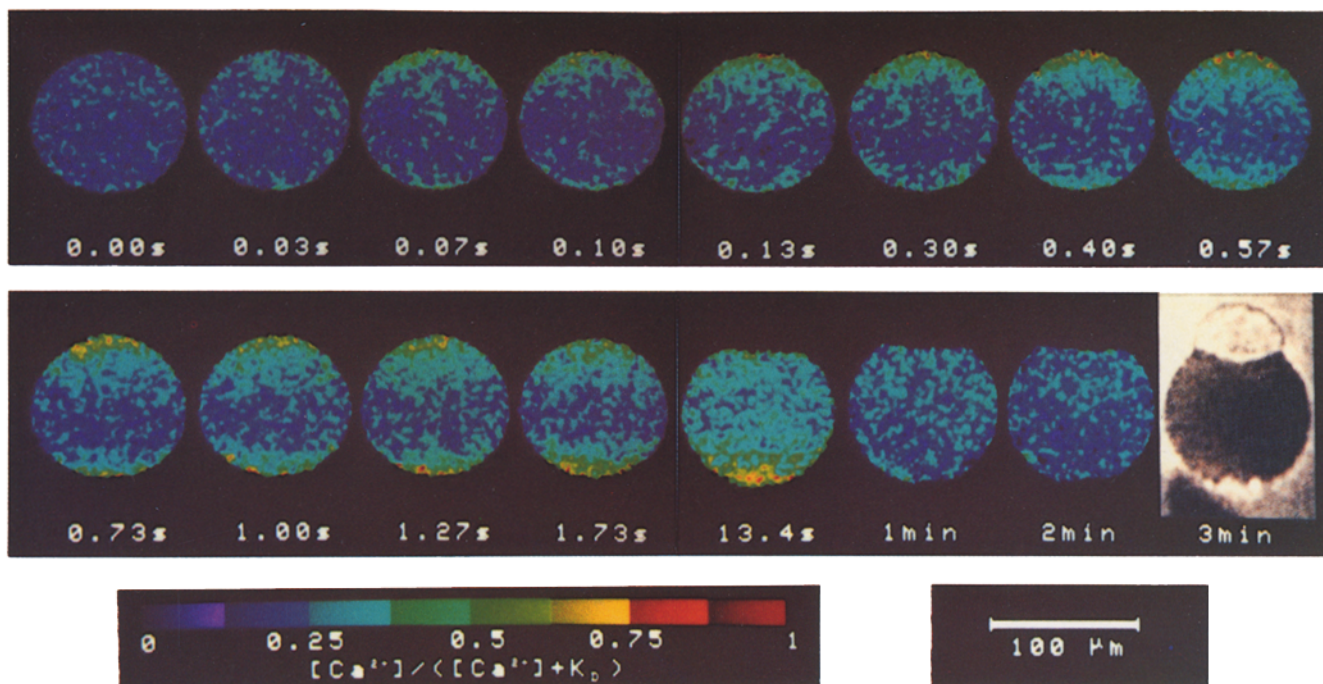
Figure 5. Snapshots, at indicated times, of Ca^{2+} influxes into an electroporated sea urchin egg. At time 0, an electric field of 400 V/cm, in the direction from top to bottom in the figure, was applied for 400 μs. Fluorescence was excited at 340 nm, and emissions above and below 455 nm were separately imaged by W color microscopy. To construct the color bar, egg homogenates containing excess $CaCl_2$ or EGTA were used as references. The dissociation constant, K_d, of indo-1 for Ca^{2+} in the egg is unknown; for a physiological saline, K_d = 0.25 μM (Grynkiewicz et al., 1985).

one. Our results suggest that the asymmetry is quantitative rather than all-or-none; at least part of the quantitative difference is in the resealing kinetics.

Conclusion

We have shown that a straightforward, inexpensive modification of an ordinary microscope makes possible the simultaneous acquisition of various kinds of spectroscopic information in every pixel of a microscope image. Furthermore, the technique is fully compatible with a variety of excitation and detection devices. The additional information provided by W microscopy will greatly help characterize transient events of interest in cell biology.

References

Axelrod, D. 1979. Carbocyanine dye orientation in red cell membrane studied by microscopic fluorescence polarization. *Biophys. J.* 26:557-574.

Foskett, J. K. 1988. Simultaneous Nomarski and fluorescence imaging during video microscopy of cells. *Am. J. Physiol.* 255:C566-C571.

Grynkiewicz, G., M. Poenie, and R. Y. Tsien. 1985. A new generation of Ca^{2+} indicators with greatly improved fluorescence properties. *J. Biol. Chem.* 260:3440-3450.

Harada, Y., A. Noguchi, A. Kishino, and T. Yanagida. 1987. Sliding movement of single actin filaments on one-headed myosin filaments. *Nature (Lond).* 326:805-808.

Herman, B., and K. Jacobson, editors. 1990. Optical Microscopy for Biology. Wiley-Liss, New York. 658 pp.

Hibino, M., M. Shigemori, H. Itoh, K. Nagayama, and K. Kinosita, Jr. 1991. Membrane conductance of an electroporated cell analyzed by submicrosecond imaging of transmembrane potential. *Biophys. J.* 59:209-220.

Hirano, K., and M. Ishikawa. 1979. Induction of aster formation and cleavage in eggs of the sea urchin *Hemicentrotus pulcherrimus* by injection of sperm components. *Dev. Growth Differ.* 21:473-481.

Huxley, A. F., and R. M. Simmons. 1972. Mechanical transients and the origin of muscular force. *Cold Spring Harbor Symp. Quant. Biol.* 37:669-680.

Inoué, S. 1986. Video Microscopy. Plenum Publishing Corp., New York. 584 pp.

Itoh, H., M. Hibino, M. Shigemori, M. Koishi, A. Takahashi, T. Hayakawa, and K. Kinosita, Jr. 1990. Multi-shot pulsed laser fluorescence microscope system. *Proc. SPIE (Soc. Photo Opt. Instr. Eng).* 1204:49-53.

Kinosita, K., Jr., S. Kawato, and A. Ikegami. 1977. A theory of fluorescence polarization decay in membranes. *Biophys. J.* 20:289-305.

Kinosita, K., Jr., S. Ishiwata, H. Yoshimura, H. Asai, and A. Ikegami. 1984. Submicrosecond and microsecond rotational motions of myosin head in solution and in myosin synthetic filaments as revealed by optical anisotropy decay measurements. *Biochemistry.* 23:453-467.

Kinosita, K., Jr., I. Ashikawa, N. Saita, H. Yoshimura, H. Itoh, K. Nagayama, and A. Ikegami. 1988. Electroporation of cell membrane visualized under a pulsed-laser fluorescence microscope. *Biophys. J.* 53:1015-1019.

Masai, J., S. Ishiwata, and S. Fujime. 1986. Dynamic light-scattering study on polymerization process of muscle actin. *Biophys. Chem.* 25:253-269.

Mehle, W., U. Zimmermann, and R. Hampp. 1985. Evidence for asymmetrical uptake of fluorescent dyes through electro-permeabilized membranes of *Avena* mesophyll protoplasts. *FEBS (Fed. Eur. Biochem. Soc.) Lett.* 185:89-94.

Neumann, E., A. E. Sowers, and C. A. Jordan, editors. 1989. Electroporation and Electrofusion in Cell Biology. Plenum Publishing Corp., New York. 436 pp.

Prochniewicz-Nakayama, E., T. Yanagida, and F. Oosawa. 1983. Studies on conformation of F-actin in muscle fibers in the relaxed state, rigor, and during contraction using fluorescent phalloidin. *J. Cell Biol.* 97:1663-1667.

Rossignol, D. P., G. L. Decker, W. J. Lennarz, T. Y. Tsong, and J. Teissie. 1983. Introduction of calcium-dependent, localized cortical granule break-down in sea-urchin eggs by voltage pulsation. *Biochim. Biophys. Acta.* 763: 346–355.

Sowers, A. E. 1988. Fusion events and nonfusion contents mixing events induced in erythrocyte ghosts by an electric pulse. *Biophys. J.* 54:619–626.

Spring, K. R. 1990. Quantitative imaging at low light levels: Differential interference contrast and fluorescence microscopy without significant light loss. *In* Optical Microscopy for Biology. B. Herman and K. Jacobson, editors. Wiley-Liss, New York. 513–522.

Taylor, D. L., A. S. Waggoner, F. Lanni, R. F. Murphy, and R. R. Birge, editors. 1986. Applications of Fluorescence in the Biomedical Sciences. Alan R. Liss, New York. 639 pp.

Toyoshima, Y. Y., S. J. Kron, E. M. McNally, K. R. Niebling, C. Toyoshima, and J. A. Spudich. 1987. Myosin subfragment-1 is sufficient to move actin filaments *in vitro. Nature (Lond.).* 328:536–539.

Tsien, R. Y. 1988. Fluorescence measurement and photochemical manipulation of cytosolic free calcium. *Trends Neurosci.* 11:419–424.

Tsong, T. Y. 1983. Voltage modulation of membrane permeability and energy utilization in cells. *Biosci. Rep.* 3:487–505.

Weeds, A. G., and B. Pope. 1977. Studies on the chymotryptic digestion of myosin. Effects of divalent cations on proteolytic susceptibility. *J. Mol. Biol.* 111:129–157.

Zimmermann, U. 1982. Electric field-mediated fusion and related electrical phenomena. *Biochim. Biophys. Acta.* 694:227–277.